
AN INPUT-TO-STATE SAFETY APPROACH TO ANOMALY-RESILIENT PARABOLIC PDEs: APPLICATION TO CYBER-PHYSICAL BATTERY MODULES

A PREPRINT

Tanushree Roy, Ashley Knichel and Satadru Dey*

January 10, 2022

ABSTRACT

Distributed Parameter Cyber-Physical Systems (DPCPSs), modelled by Partial Differential Equations (PDEs), are increasingly vulnerable to anomalies such as physical faults as well as cyber-attacks. This motivates the need for strategies towards anomaly-resilient control of these systems. Although anomaly detection and diagnostics in PDE systems have received considerable attention in existing literature, fault-tolerant or anomaly-resilient control for PDEs remains relatively under-explored. However, given the vulnerabilities of these systems against anomalies, it is essential that the control systems possess resilience against these disruptions. In this context, we explore a Practical Input-to-Safety (pISSf) based control design approach for a class of DPCPSs modelled by linear Parabolic PDEs. Specifically, we develop a design framework for anomaly-resilient control for this class of system with both safety and stability guarantees based on control Lyapunov functional and control barrier functional. To illustrate our methodology, we apply our strategy to design a thermal-anomaly resilient boundary coolant control system for a cyber-physical battery module. Several simulation studies are done to show the efficacy of our method under anomalies such as mechanical battery degradation and cyber-attack mediated overdischarge.

1 Introduction

Many modern distributed parameter systems consist of wide-spread interconnections among their physical and cybernetic components, and are considered as Distributed Parameter Cyber-Physical Systems (DPCPSs). As a consequence, the vulnerability of these systems to anomalies such as physical faults and cyberattacks has increased considerably. This necessitates the design of controllers for such DPCPSs to be resilient against these anomalies. In this work, we explore control design of anomaly-resilient DPCPSs modelled by linear parabolic PDEs utilizing the practical Input-to-State Safety (pISSf) framework. We illustrate this approach by focusing on the application of thermal anomaly-resilient cyber-physical battery systems.

Stability and safety verification in Ordinary Differential Equations (ODEs) has been explored widely and detailed list of works can be found in survey papers [1] and [2]. Input-to-State Stability (ISSt) in sense of Sontag has been investigated using Lyapunov functionals [3]. The notion of practical ISSt (pISSt) has been explored in [3] that augments the original ISSt with certain practical considerations. On the other hand, Input-to-State Safety (ISSf) was introduced in [4]. Since then, two prominent methods are generally used for ISSf analysis/design/verification: reachable sets approximation [5–7] and barrier functionals [8–11]. Among the various works in this domain, [12, 13] introduces a notion of practical Input-to-State Safety (pISSf) in conjunction with pISSt with guaranteed safety for affine nonlinear ODEs using barrier functionals.

Similar to ODEs, notions of ISSt for PDE systems have garnered a lot of attention recently (see survey paper [14]). For example, PDE ISSt have been explored for reaction-diffusion systems [15], hyperbolic systems [16], [17], parabolic

*T. Roy, A. Knichel and S. Dey are with the Department of Mechanical Engineering, The Pennsylvania State University, University Park, Pennsylvania 16802, USA. {tbr5281, ark5514, skd5685}@psu.edu.

systems [18], parabolic PDE systems with boundary disturbances [19], [20], systems with distributed time-delays [21], and diffusion equation with time-varying distributed coefficients [22]. Notions of practical Input-to-State Stability (pISS) for PDEs have been explored in [23]. In contrast to ISS, ISSf has remained mostly unexplored in the context of PDEs. In [24], safety verification using barrier functionals for homogeneous distributed parameter systems has been considered. In this work, numerical strategies based on semi-definite programming has been used for the construction of barrier functionals. However, control performance under anomalies has not been considered in this work. Given the importance of maintaining system safety under physical faults or cyber-attacks, it is critical to consider control system design for PDE systems under these anomalies.

Control of PDE systems has been widely explored over the years [25–30] while anomaly (such as fault or cyber-attack) detection in PDE systems has also received considerable attention [17, 18, 31–40]. However, anomaly-resilient and fault-tolerant control of PDE systems has remained relatively under-explored in existing literature. Over the past few years, some works have been presented on this particular topic. For example, fault-tolerant control for distributed process and transport-reaction processes are considered in [41] and [42], respectively. For a quasi-linear parabolic PDE, [43] proposed a model-based actuator fault detection and a supervisory fault-tolerant control to engage different actuator configuration in the event of fault. In [44], an actuator-fault agnostic control strategy has been proposed for flexible aircraft wing systems using adaptive control laws. Furthermore, an observer-based fuzzy fault-tolerant controller have been developed for a class of nonlinear DPCPS in [45]. In [46], fault-tolerant control design has been presented for interconnected linear hyperbolic PDE systems. Fault-tolerant control for a class of switched parabolic systems is considered in [47]. Boundary adaptive fault-tolerant control for a flexible timoshenko arm is explored in [48]. In [32], actuator fault management is explored for uncertain parabolic PDEs. [49] proposed an active fault-tolerant control for a highly dissipative nonlinear system under actuator faults by approximating the PDE by its finite-dimensional dominant dynamics and through sampled sensor data. In [50], a backstepping-based decentralized actuator fault-tolerant controller have been developed for hypersonic vehicles, modeled as coupled PDE and ODE. Although these approaches presented interesting and useful results, the idea of Input-to-State Safety remains unexplored in the context of PDE system fault-tolerance, to the best of our knowledge. Input-to-State Safety techniques can provide explicit safety guarantee in the PDE systems under exogenous anomalies. Especially, such design can ensure that the PDE system states remain inside the safe region even in the presence of anomalies. In this work, we address this gap and explore such Input-to-State Safety framework to design anomaly-resilient controller for linear parabolic PDE systems with an application to thermal management of cyber-physical battery modules.

Battery systems are becoming omnipresent in many applications including electric transportation, renewable energy, medical devices, smart buildings, and consumer electronics. Modern battery systems exhibit cyber-physical nature, for example, wireless Battery Management System [51] and cloud-connected batteries [52]. Enabling safety and security of these modern battery systems are essential in order to accelerate electrification. Anomalies in battery systems pose significant safety and security risks leading to potential loss of lives and properties. These anomalies can either arise from physical faults or they can be caused by adversarial cyber-attacks where the adversary manipulates communicated signals to induce a disastrous outcome. Accordingly, these modern battery systems must be equipped with measures to handle such anomalies. In this work, we focus on battery module thermal management and propose a safety framework utilizing PDE pISSf and ISS techniques.

Thermal management for battery cells has been studied in existing literature. For example, thermal fault-tolerant control is presented in [53] where a fault and internal state estimator was used in conjunction with a feedback control law derived from certain optimal criteria. However, this approach focuses on single battery cells and utilize lumped thermal models. Active control based battery module thermal management has been studied in [54]. However, this approach utilizes lumped cell-level thermal models and does not consider presence of anomalies. Furthermore, these thermal control approaches may not be readily applicable to module-level thermal control due to complex spatiotemporal thermal dynamics and inter-cell thermal coupling in the modules. A few other thermal management studies on battery modules or module exist [55–57]. However, these approaches do not consider control under the presence of anomalies. As discussed before, it is essential to ensure battery systems are resilient against anomalies such as physical faults and cyber-attacks. Accordingly, thermal management of battery modules should consider the inevitable presence of these anomalies. In this context, we propose a thermal management strategy for battery modules under anomalies such as physical faults or cyber-attacks.

In light of the aforementioned discussion, the main contributions of this paper are the following: (1) *Building upon the existing literature, we extend PDE pISSf techniques by considering control design under exogenous anomalies.* (2) *We propose a thermal control approach for battery modules under anomalies by combining PDE thermal model, PDE pISSf and ISS techniques.* In this framework, we consider a one-dimensional thermal PDE model for a battery module with a boundary coolant control. Next, we construct a control barrier functional and control Lyapunov functional for obtaining analytical guarantees for safety and stability for the battery system. The analytical guarantees allows us design the controller gains for actuating the boundary coolant.

The rest of the paper is organized as follows. Section 2 sets up the problem by discussing the battery module thermal model and formulating control objectives. Sections 3 and 4 detail the pISSf-ISSf framework. Section 4 presents case studies to illustrate the proposed framework. Finally, Section 5 concludes the paper.

2 Problem Setup - Anomaly-resilient Linear Parabolic PDEs

In this work, we consider a DPCPS where the physical system is modeled by a linear Parabolic PDE while the controller lies in the cyber layer. Anomalies in DPCPS systems can be due to internal degradations or faults in the physical plant or cyber-attacks such as corruption of command signals via compromised communication channel between the cybernetic command center and physical plant. The class of linear parabolic PDEs we focus in this work is given by

$$T_t(x, t) = \alpha T_{xx}(x, t) + Q(x, t) + \Delta(x, t), \quad (1)$$

where $\alpha > 0$, $T(x, t)$ is the solution of the PDE over time $t \in (0, t_{max})$, $0 < t_{max} < \infty$ and space $x \in [0, L]$ with known distributed input $Q(x, t)$ and anomaly $\Delta(x, t)$. In this work, we consider Robin-type boundary condition (which can be regarded as a weighted sum of Neumann and Dirichlet conditions) given by

$$m_1 T_x(0, t) + m_2 T(0, t) = f_1(t), \quad (2)$$

$$m_3 T_x(L, t) + m_4 T(L, t) = f_2(t), \quad (3)$$

where $m_i, i \in \{1, 2, 3, 4\}$ are known parameters and $f_1(t)$ and $f_2(t)$ are the boundary control inputs. Finally, the initial condition for the system is given by $T(x, 0) = T_0$. The above framework can be applied to various DPCPSs including battery modules. Subsequently, we present how thermal model for battery modules can be modeled as (1) with similar Robin-type boundary condition to motivate our work in this class of linear parabolic PDEs.

2.1 A Mathematical Model of Battery Module Thermal Dynamics

The battery module considered here consists of multiple cells that are stacked together to provide certain electrical power output. As current flows during charging and discharging, heat generation in battery cells and their interconnections cause temperature rise. Coolant channels are placed in the system to cool down the battery module. From a thermal management viewpoint, we attempt to maintain the battery module temperature around a desired safe temperature by controlling the temperature of the coolant fluid at the boundary. Figure 1 shows the schematic of thermal management scheme.

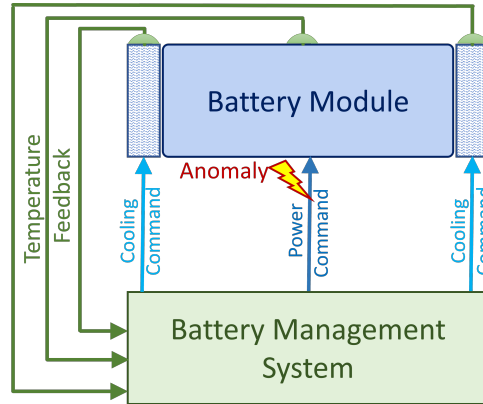


Figure 1: Safe and secure thermal management scheme for battery module.

In order to capture thermal distribution of heat in battery module, we use the one-dimensional heat PDE given by (1) (please refer to [58], [59], [60], and [61] for details of the modeling). Here $T(x, t)$ is the distributed temperature of the module, $\alpha = \frac{k_b}{\rho_b c_{p,b}}$ is the thermal conductivity, $Q = \frac{I^2(x, t)R}{\rho_b c_{p,b} V_b}$ is the internal distributed heat generation in the battery module due to nominal current flow with R being the resistance of the battery and $I(x, t)$ being the battery module current, and V_b represents volume of the module. The variable $\Delta(x, t)$ represent an unknown anomaly affecting the module temperature. Additionally, ρ_b , $c_{p,b}$ and k_b represent the equivalent density, specific heat capacity and thermal conductivity of the battery, respectively.

As mentioned in the introduction, the anomaly $\Delta(x, t)$ can be originated due one of the following causes:

- **Physical faults:** These faults can be caused by internal electrochemical reactions such as dendrite growth, thermal and mechanical abuse of batteries, and internal/external short circuits. Many of these physical causes ultimately exhibit themselves as thermal anomalies in the battery, often in the form of abnormal heat generation. For details of these physical failure modes, please refer to [62–64]. In this case, the physical fault will show up as $\Delta(x, t) = \frac{Q_a(x, t)}{\rho_b c_{p, b} V_b}$ where Q_a is the abnormal heat generation.
- **Cyber-attacks:** Cyber-attacks can be induced by adversaries by manipulating the data through the communication network. For example, the current command $I(x, t)$ to the battery system through the Controller Area Network (CAN) bus can be modified to overcharge or overdischarge the battery. This could be particularly dangerous in case of wireless Battery Management System [51] or cloud-connected batteries [52]. In this case, the cyber-attack will show up as an additive or multiplicative type anomaly, i.e. $I(x, t) + I_a$ or $a_a I(x, t)$ where I_a and a_a represent attack type anomalies.

Note that the objective of this work is not to distinguish the cause of anomaly (that is, whether it is a physical fault or cyber-attack), but to ensure thermal safety in the presence of these anomalies.

In our problem framework, there is convection heat transfer between the coolant and the module at the two sides [59]. It is assumed that the heat resistance through the coolant channel wall is negligible. This results in Robin-type boundary conditions as shown below:

$$T_x(0, t) = k(T(0, t) - T_{c1}(t)), \quad (4)$$

$$T_x(L, t) = k(T_{c2}(t) - T(L, t)), \quad (5)$$

where coefficient $k = \frac{\eta}{k_b}$, parameter η denotes the coolant heat transfer coefficient, temperatures $T_{c1}(t)$ and $T_{c2}(t)$ represent the coolant temperatures at the the ends of the battery module.

In terms of output measurements, temperature sensors are placed along the length of the battery module. In this work, we assume that we have sensors are placed in each boundary, and an additional sensor is placed in the middle of the module. That is, $T(0, t)$, $T(L, t)$, and $T(m, t)$ are measured where m is a middle point, i.e. $0 < m < L$.

Remark 1. It is important to note that $Q(x, t)$ in (1) is treated as a not controllable but known input whereas the coolant temperatures $T_{c1}(t)$ and $T_{c2}(t)$ in (4) and (5) are chosen as control inputs acting on the boundary of the battery module. The nominal heat $Q(x, t)$ is treated as not controllable as this is generated based on the current profile determined by the power requirement of the battery system. For example, in an electrified vehicle such current profile is determined by the driver's acceleration and brake pedal inputs, which are generally not controlled by the thermal management system.

2.2 Battery Thermal Management - Control Problem Formulation

Effective thermal management requires maintaining the temperature along the battery module close to a desired safe temperature, that is $|T(x, t) - T_d|$ should be as small as possible, where T_d is a predetermined desired safe temperature. In this work, we further characterize this objective in terms of pISSf and ISSt properties. First, we write the error system PDE as

$$h_t(x, t) = \alpha h_{xx}(x, t) + D(x, t) + u(x, t), \quad (6)$$

$$h_x(0, t) = k[h(0, t) - u_1(t)], \quad (7)$$

$$h_x(L, t) = k[u_2(t) - h(L, t)], \quad (8)$$

where $h(x, t) = T(x, t) - T_d$ is the error with respect to the desired safe temperature, $u = Q$ is the heat generation, and u_1 and u_2 are boundary cooling inputs. Here D represents the anomaly (effect of $\Delta(x, t)$ in (1)). In this work, we choose the following structures of the boundary cooling control inputs:

$$u_1(t) = \mu_1 h(0, t) + \mu_2 h_t(0, t) + \mu_3 h(m, t), \quad (9)$$

$$u_2(t) = \beta_1 h(L, t) + \beta_2 h_t(L, t) + \beta_3 h(m, t), \quad (10)$$

where μ_i and β_i with $i \in \{1, 2, 3\}$ are the control gains. This modifies the boundary condition to

$$h_x(0) = k[(1 - \mu_1)h(0) - \mu_2 h_t(0) - \mu_3 h(m)], \quad (11)$$

$$h_x(L) = k[(\beta_1 - 1)h(L) + \beta_2 h_t(L) + \beta_3 h(m)]. \quad (12)$$

Subsequently, our goal is to design these gains such that the following two properties are satisfied:

- **Practical Input-to-State Safety (pISSf)** with respect to an unsafe set \mathcal{U} , which is defined by the following criterion on the system state $h(x, t)$ [12]:

$$|h|_{\mathcal{U}}^2 \geq \bar{k}_1 |h_0|_{\mathcal{U}}^2 - \bar{k}_2 e^{\bar{k}_3 t} \|u\|_{\infty}^2 - \bar{k}_4 e^{\bar{k}_5 t} \|D\|_{\infty}^2 - \bar{k}_6 e^{\bar{k}_7 t}, \quad (13)$$

where $|\cdot|_{\mathcal{U}}$ denotes a distance metric from the unsafe set; $\|\cdot\|_{\infty}$ denotes the L^{∞} norm given by $\|M\|_{\infty} = (ess) \sup_{t \in (0, T)} \|M(x, t)\|_2^2$; $\|\cdot\|_2$ denotes the L^2 spatial norm given by $\sqrt{\int_0^L M^2(x, t) dx}$; $h_0 = h(\cdot, 0)$ is the initial condition for (6); u and D are the in-domain nominal input and the anomaly, respectively; and $\bar{k}_i, i \in \{1, \dots, 7\}$ are positive constants.

- **Input-to-State Stability (ISSt)** which is defined by the following criterion on the system state $h(x, t)$ [12, 23]:

$$\|h\|_S^2 \leq \tilde{k}_1 e^{-\tilde{k}_2 t} \|h_0\|_S^2 - \tilde{k}_3 e^{-\tilde{k}_4 t} \|u\|_{\infty}^2 - \tilde{k}_5 e^{-\tilde{k}_6 t} \|D\|_{\infty}^2 - \tilde{k}_7 e^{-\tilde{k}_8 t}, \quad (14)$$

where $\|h\|_S$ is some spatial norm in $[0, L]$ (defined here as $\|h\|_S := \sqrt{\int_0^L h^2 dx + h^2(L) + h^2(0)}$; $\|\cdot\|_{\infty}$ denotes the L^{∞} norm given by $\|M\|_{\infty} = (ess) \sup_{t \in (0, T)} \|M(x, t)\|_2$; $h_0 = h(\cdot, 0)$ is the initial condition for (6); u and D are the in-domain nominal input and the anomaly, respectively; and $\tilde{k}_i, i \in \{1, \dots, 8\}$ are positive constants.

In the subsequent sections, our approach of finding the control gains are as follows. First, in Section 3, we find the conditions on control gains that satisfy the pISSf criterion in (13). Next, in Section 4, we find the additional conditions on control gains for which the system is ISSt in the sense of (14) - in addition to being pISSf.

3 Input-to-State Safety Criteria for Battery Thermal Management

In this section, we focus on the Input-to-State Safety condition mentioned in (13). First, we formulate the unsafe set \mathcal{U} and the distance metric $|h|_{\mathcal{U}}$. Subsequently, we construct a control barrier functional that would eventually help us derive the conditions on control gains to satisfy (13).

3.1 Unsafe Set Formulation

The goal of this work is to design a control strategy that will guarantee safety of the battery system under anomalies. The criterion for safety is that the maximum temperature deviation of the battery from a set-point remains below a prescribed threshold h_{max} . Mathematically, this implies

$$\max_{x \in [0, L]} |h(x, t)| \leq h_{max}, \forall x \in [0, L], t \in (0, t_{max}). \quad (15)$$

Alternatively, we can define an unsafe set

$$\mathcal{U} = \{a \in \mathbb{R} : a > h_{max}\}, \quad (16)$$

such that $\max_{x \in [0, L]} |h(x, t)| \leq a, \forall x \in [0, L], \forall a \in \mathcal{U}, t \in (0, t_{max})$. Since, this max function is not continuous, it is a poor candidate for constructing the safety barrier functional. Thus, we use the following Lemma to obtain a majorizing continuous function which when remains below the h_{max} guarantees safety for the system (6). This Lemma is a modified form obtained from the standard Agmon's Inequality [27].

Lemma 1 (Modified Agmon's Inequality). *For any function $h(x, \cdot)$ in the Sobolev space, the following inequality hold*

$$\max_{x \in [0, L]} |h(x, \cdot)|^2 \leq \int_0^L \left(h^2(x, \cdot) + h_x^2(x, \cdot) \right) dx + h^2(m). \quad (17)$$

Proof. For some $0 < m < x < L$, it is straightforward to prove that $\int_m^x h h_x dx = \frac{1}{2} (h^2(x, \cdot) - h^2(m, \cdot))$. With further simplification, this yields

$$h^2(x, \cdot) \leq 2 \int_m^L |h| |h_x| dx + h^2(m). \quad (18)$$

Next extending the limit of the integral for a positive valued function to $[0, L]$ and using Young's Inequality, we obtain

$$h^2(x, \cdot) \leq \int_0^L (h^2 + h_x^2) dx + h^2(m). \quad (19)$$

Since, the right-hand side of the inequality is independent of x , we obtain (17). \blacksquare

Lemma 1 suggests that if $\int_0^L (h^2 + h_x^2) dx + h^2(m) \leq h_{max}^2$, then the maximum temperature variation over the whole spatial domain will remain below the maximum prescribed temperature deviation h_{max} . Keeping this criterion in mind, let us define the distance metric for our framework.

For a given function $h \in C([0, L] \times (0, t_{max}))$ with $t_{max} > 0$, we define the distance of $h(x, t)$ from an unsafe set $\mathcal{U} \in \mathbb{R}$ by the following metric:

$$|h|_{\mathcal{U}} := \min_{a \in \mathcal{U}} \left\{ a^2 - \left[\int_0^L \left(h^2(x, \cdot) + h_x^2(x, \cdot) \right) dx + h^2(m) \right] \right\}^{\frac{1}{2}}. \quad (20)$$

3.2 Practical Input-to-State Safety via ISSf Barrier Functional

It can be shown that the existence of a particular ISSf barrier functional can automatically guarantee pISSf in the sense of (13) [12]. For the sake of completeness, we present the following proposition which is similar to the one presented in [12]. The only difference between the conditions in [12] and the following is that the parameter κ appears in Condition 1 in [12] whereas it appears in Condition 2 in the following.

Proposition 1. *Consider the PDE system given by (6)-(10), the prescribed unsafe set \mathcal{U} given by (16) and the distance metric as defined in (20). Suppose there exists a safety barrier functional $\mathcal{B} : \mathbb{H}_1 \rightarrow \mathbb{R}$ satisfying the following two conditions:*

Condition 1: $-c_1|h|_{\mathcal{U}}^2 \leq \mathcal{B}(h) \leq -c_2|h|_{\mathcal{U}}^2$

Condition 2: $\dot{\mathcal{B}}(h) \leq -c_3|h|_{\mathcal{U}}^2 + c_4\|D\|^2 + c_5\|u\|^2 + \kappa$ where $\dot{\mathcal{B}}(h)$ is the derivative of the ISSf barrier functional \mathcal{B} along the solution trajectory $h(x, t)$ of the PDE system, constants $c_i, \forall i \in \{1, 2, 3, 4, 5\}$ and κ are positive constants. Then the PDE system (6) is considered to be practical Input-to-State safe with respect to the unsafe set \mathcal{U} .

Proof. This proof can be done by following the approach shown in [12]. ■

According to the above proposition, if we can construct a safety barrier functional \mathcal{B} , we can guarantee the pISSf property for the PDE system given in (6). Let us now construct an ISSf barrier functional \mathcal{B} that satisfies the two conditions presented in Proposition 1.

3.3 Construction of ISSf Barrier Functional

We construct the ISSf barrier functional in the following way:

$$\mathcal{B}(h) = \int_0^L \left(h^2(x, \cdot) + h_x^2(x, \cdot) \right) dx + h^2(m) - h_{max}^2. \quad (21)$$

With this, in the following Theorem, we show that the control barrier function given by (21) guarantee pISSf in the sense of (13) by satisfying the two conditions presented in Proposition 1.

Theorem 1 (Design Requirements for ISSf). *Consider the system (6) with boundary conditions (11)-(12). Let us also consider the unsafe set for this system to be (16), the metric measuring the distance from this unsafe set to be given by (20) and a barrier functional (21) for this system. If the controller gains are chosen as*

$$\mu_1 < 1, \frac{(\mu_1 - 1)}{\alpha} \leq \mu_2 < 0, \mu_3 < 0, \quad (22)$$

$$\beta_1 < 1, \frac{(\beta_1 - 1)}{\alpha} \leq \beta_2 < 0, \beta_3 < 0, \quad (23)$$

and there exist constants $c_i, i \in \{1, \dots, 5\}$ such that

$$\begin{aligned} c_1 &> 1, 0 < c_2 < 1, \\ c_3 &= 2 \max \left\{ \alpha, \left(\frac{\gamma_1}{2} + \frac{\gamma_2}{2} \right), \frac{\gamma_5}{2} + \frac{k\alpha}{4} \left[\frac{\mu_3^2}{(1 - \mu_1)} + \frac{\beta_3^2}{(1 - \beta_1)} \right] \right\}, \\ c_4 &= \frac{1}{\gamma_1} + \frac{1}{\gamma_3}, \quad c_5 = \frac{1}{\gamma_2} + \frac{1}{\gamma_4}, \end{aligned} \quad (24)$$

where the design parameters $\gamma_1 > 0, \gamma_2 > 0$, and the design parameters γ_3, γ_4 and γ_5 satisfy the following condition

$$\frac{\gamma_3 + \gamma_4}{2\alpha^2} + \frac{1}{\gamma_5} < \frac{1}{\alpha}; \quad (25)$$

then the system (6) satisfies the two conditions of Proposition 1 with $\kappa = h_{max}c_3$, and is considered to be practical Input-to-State Safe (pISSf) with respect to the unsafe set \mathcal{U} .

Proof. First, we will prove that the barrier functional (21) satisfies Condition 1 from Proposition 1. Considering (16), we can observe that

$$h_{max}^2 - \left(\int_0^L \left(h^2(x, \cdot) + h_x^2(x, \cdot) \right) dx + h^2(m) \right) = \min_{a \in \mathcal{U}} \left[a^2 - \left(\int_0^L \left(h^2(x, \cdot) + h_x^2(x, \cdot) \right) dx + h^2(m) \right) \right]. \quad (26)$$

Consequently, using (26) in (21), we can re-write $\mathcal{B}(h)$ as

$$\mathcal{B}(h) = - \min_{a \in \mathcal{U}} \left[a^2 - \left(\int_0^L \left(h^2(x, \cdot) + h_x^2(x, \cdot) \right) dx + h^2(m) \right) \right], \quad (27)$$

$$\implies \mathcal{B}(h) = -|h|_{\mathcal{U}}^2, \quad (28)$$

where $|h|_{\mathcal{U}}$ is the distance metric in (20). From (28), we can write the following two inequalities:

$$\mathcal{B}(h) \geq -c_1|h|_{\mathcal{U}}^2, \quad \mathcal{B}(h) \leq -c_2|h|_{\mathcal{U}}^2, \quad (29)$$

where $c_1 > 1$ and $0 < c_2 < 1$ are two constants. This confirms that $\mathcal{B}(h)$ satisfies Condition 1 from Proposition 1.

Next, we will prove that the barrier functional (21) satisfies Condition 2 from Proposition 1. In order to do so, we take the derivative of (21) along the trajectory of solution of $h(x, t)$ to obtain:

$$\dot{\mathcal{B}}(h) = 2 \left[\int_0^L (hh_t + h_x h_{xt}) dx + h(m)h_t(m) \right]. \quad (30)$$

Subsequently, we replace h_t and $(h_t)_x$ using (6), and further using integration by parts we have

$$\dot{\mathcal{B}}(h) = BT_1 - \alpha \int_0^L h_x^2 dx + \int_0^L hD dx + \int_0^L hu dx - \int_0^L h_{xx}h_t dx + h(m)h_t(m), \quad (31)$$

where BT_1 represents the boundary terms given by

$$BT_1 = h_x(L)(\alpha h(L) + h_t(L)) - h_x(0)(\alpha h(0) + h_t(0)). \quad (32)$$

By replacing $h_x(0)$ and $h_x(L)$ from (11) and (12), respectively, and choosing $\frac{(\mu_1-1)}{\alpha} \leq \mu_2 < 0$ and $\frac{(\beta_1-1)}{\alpha} \leq \beta_2$, (32) yields:

$$BT_1 \leq \frac{k\alpha}{4} \left[\frac{\mu_3^2}{(1-\mu_1)} + \frac{\beta_3^2}{(1-\beta_1)} \right] h^2(m). \quad (33)$$

In (31), replacing h_{xx} with (6), using the upper bound of BT_1 from (33), and using Young's inequality, we obtain:

$$\dot{\mathcal{B}}(h) \leq -c_3|h|_{\mathcal{U}}^2 + c_4\|D\|^2 + c_5\|u\|^2 + \kappa, \quad (34)$$

where c_3 , c_4 , and c_5 are given by (24) and $\kappa = h_{max}c_3$. The design parameters $\gamma_1 > 0$, $\gamma_2 > 0$, and the design parameters γ_3 , γ_4 and γ_5 are chosen such that (25) is satisfied. ■

In this section, we have derived the conditions on control gains for which the system is pISSf. In the following section, we will find additional conditions on control gains for which the system is ISSf - in addition to being pISSf.

4 Input-to-State Stability Criteria for Battery Thermal Management

In the present section, we will show that the control gain conditions in Theorem 1, along with certain additional conditions, simultaneously satisfy the practical Input-to-State Safety (pISSf) criterion in the sense of (13) and Input-to-State Stability (ISSf) criterion in the sense of (14). In order to do so, we consider the following control Lyapunov functional for a PDE system (6):

$$V(h) = \frac{1}{2} \left[\int_0^L h^2 dx + \beta_4 h^2(0) + \beta_5 h^2(L) \right], \quad (35)$$

where $\beta_4 > 0$ and $\beta_5 > 0$. Following the results in existing literature [65], we can say that if there exists a functional $V(h)$ for an infinite dimensional system, which satisfies the following two conditions:

$$d_1 \|h\|_S^2 \leq V(h) \leq d_2 \|h\|_S^2, \quad (36)$$

$$\dot{V}(h) \leq -d_3 V(h) + d_4 \|D\|^2 + d_5 \|u\|^2, \quad (37)$$

where $d_i, \forall i \in \{1, 2, 3, 4, 5\}$ are positive constants, then system is ISSt. In our formulation, the norm is defined as $\|h\|_S := \sqrt{\int_0^L h^2 dx + h^2(L) + h^2(0)}$ and $\|\cdot\|$ is the spatial L^2 norm.

Before presenting the theorem that provides the design specifications for ensuring ISSt, we will introduce a version of Poincare's Inequality through the following Lemma.

Lemma 2. *Following Poincare's Inequality [27], it can be easily shown that for the PDE system given by (6) with continuously differentiable solution on $x \in [0, L]$, the following is true*

$$-\int_0^L h_x^2 dx \leq \frac{1}{4} \left[h^2(0) + h^2(L) - 2 \int_0^L h^2 dx \right]. \quad (38)$$

With this we will present the theorem which prescribes the design requirements on the controller gains in order to guarantee both pISSf and ISSt for the PDE system (6)-(10).

Theorem 2 (Design Requirements for both pISSf and ISSt). *Consider the system (6) with boundary conditions (11)-(12). If there exists controller gains that satisfy (22)-(23) and the following additional conditions:*

$$\tilde{d}_2 := k\alpha(1 - \mu_1) - \frac{\alpha}{4} - \frac{k\alpha\mu_3}{2\sigma_3} > 0, \quad (39)$$

$$\tilde{d}_3 := k\alpha(1 - \beta_1) - \frac{\alpha}{4} - \frac{k\alpha\beta_3}{2\sigma_4} > 0, \quad (40)$$

where the design parameters $\sigma_i > 0, i \in \{1, 2, 3, 4\}$ are chosen such that

$$\tilde{d}_1 := \alpha - (\sigma_1 + \sigma_2 + k\alpha(\mu_3\sigma_3 + \beta_3\sigma_4)) > 0, \quad (41)$$

then the system (6) is considered to be both pISSf and ISSt.

Proof. Let us consider the Lyapunov functional given by (35) where β_4 and β_5 are chosen as

$$\beta_4 = -k\alpha\mu_2 > 0, \quad \beta_5 = -k\alpha\beta_2 > 0, \quad (42)$$

where μ_2 and β_2 are chosen following the conditions in (22)-(23) of Theorem 1. The first condition given in (36) can be proved by choosing $d_1 = \frac{1}{2} \min\{1, \beta_4, \beta_5\} > 0$ and $d_2 = \frac{1}{2} \max\{1, \beta_4, \beta_5\} > 0$.

Next, to prove the second condition given in (37), we take the time derivative of $V(h)$ along the direction of the solution of (6). Subsequently, we apply Young's inequality to the cross terms to obtain:

$$\dot{V} = BT_2 - \alpha \int_0^L h_x^2 dx + \left(\frac{\sigma_1 + \sigma_2}{2} \right) \int_0^L h^2 dx + \frac{1}{2\sigma_1} \|D\|^2 + \frac{1}{2\sigma_2} \|u\|^2, \quad (43)$$

where σ_1 and σ_2 are positive constants, and the boundary term BT_2 is given by

$$BT_2 = h(L) (\alpha h_x(L) + \beta_4 h_t(L)) + h(0) (-\alpha h_x(0) + \beta_5 h_t(0)). \quad (44)$$

Next, in (44), $h_x(0)$ and $h_x(L)$ are replaced by boundary conditions (11)-(12). Thus, for the first term on the right hand side of (44), we obtain:

$$h(L) (\alpha h_x(L) + \beta_4 h_t(L)) = \alpha k(\beta_1 - 1)h^2(L) + (\alpha k\beta_2 + \beta_4)h(L)h_t(L) + \alpha k\beta_3 h(L)h(m), \quad (45)$$

and for the second term on the right hand side of (44), we get:

$$h(0) (-\alpha h_x(0) + \beta_5 h_t(0)) = -\alpha k(1 - \mu_1)h^2(0) + (\alpha k\mu_2 + \beta_5)h(0)h_t(0) + \alpha k\mu_3 h(0)h(m). \quad (46)$$

In (45) and (46), we note that the coefficients of terms $h(L)h_t(L)$ and $h(0)h_t(0)$ becomes zero using (42). Finally, (44) becomes:

$$BT_2 = -\alpha k(1 - \mu_1)h^2(0) + \alpha k\mu_3 h(0)h(m) - \alpha k(1 - \beta_1)h^2(L) + \alpha k\beta_3 h(L)h(m), \quad (47)$$

where μ_1, μ_3 and β_1, β_3 are chosen following the conditions in (22)-(25) of Theorem 1. Subsequently, we apply Young's Inequality to the cross-terms $h(0)h(m)$ and $h(L)h(m)$ in (47) to obtain

$$BT_2 = - \left(\alpha k(1 - \mu_1) - \frac{k\alpha\mu_3\sigma_3}{2} \right) h^2(0) - \left(\alpha k(1 - \beta_1) - \frac{k\alpha\beta_3\sigma_4}{2} \right) h^2(L) + \left(\frac{k\alpha\mu_3}{2\sigma_3} + \frac{k\alpha\beta_3}{2\sigma_4} \right) h^2(m). \quad (48)$$

Next, we use $h^2(m) < \int_0^L h^2 dx$ in (48) and substitute BT_2 in (43). Thereafter, we apply the inequality (38) in (43) to obtain

$$\dot{V} \leq - \frac{\tilde{d}_1}{2} \int_0^L h^2 dx - \tilde{d}_2 h^2(0) - \tilde{d}_3 h^2(L) + \frac{1}{2\sigma_1} \|D\|^2 + \frac{1}{2\sigma_2} \|u\|^2,$$

where \tilde{d}_1 is given in (41), \tilde{d}_2 and \tilde{d}_3 are given in (39)-(40). Finally, choosing $d_3 = 2 \min \left\{ \frac{\tilde{d}_1}{2}, \frac{\tilde{d}_2}{\beta_4}, \frac{\tilde{d}_3}{\beta_5} \right\}$, $d_4 = \frac{1}{2\sigma_1}$ and $d_5 = \frac{1}{2\sigma_2}$ we obtain (37). This implies that for the chosen controller gains using (22)-(25), the system is ISSt. Now by Theorem 1, we have already proved that these gains satisfy the pISSf condition. Thus we proved that the system is both pISSf and ISSt under the given design requirements. ■

5 Simulation Case Studies

In this section, we present some case studies to illustrate the effectiveness of the proposed framework. The battery model parameters are adopted from [59, 66, 67]. The simulation is implemented in MATLAB. In the plant model simulation, we have injected zero mean Gaussian type measurement noise ($\mathcal{N}(0, 0.1)$) in the temperature outputs as well as zero mean Gaussian type process noise ($\mathcal{N}(0, 0.01)$) in the system dynamics to capture realistic scenarios. The battery module is operated under a current profile derived from Urban Dynamometer Driving Schedule (UDDS) and the current profile is shown in Fig. 2. The desired set-point temperature here is $T_d = 298K$.

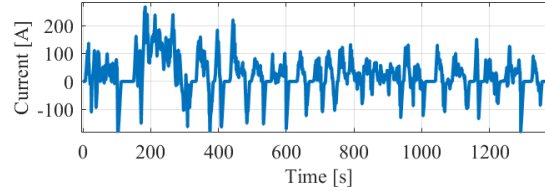


Figure 2: Battery module current profile derived from Urban Dynamometer Driving Schedule (UDDS).

To illustrate the advantages of the proposed approach, we compare the following approaches:

- **Open-loop Control (OC):** In this case, we have used a constant cooling temperature control that is not manipulated based on temperature feedback. In our case studies, the constant cooling temperature is kept at $298K$ at both the boundaries.
- **Stability-Only Control (St-C):** In this case, we have used Input-to-State Stability (ISSt) criterion to design the closed-loop control gains. The gains for St-C are calculated such that they satisfy the stability conditions (36)-(37), while they may or may not satisfy the safety conditions given in Theorem 1 (22)-(25) for unsafe temperature specified as $T > 313K$. Note that, if the design is done solely based on ISSt criterion, then there is no guarantee that it will also satisfy pISSf. To illustrate this point, and to highlight the potential advantage of combined pISSf-ISSt design, here we choose the St-C such that the gains do not satisfy pISSf conditions for the chosen unsafe set.
- **Stability-and-Safety Control (StSf-C) - Proposed Approach:** We have used both practical Input-to-State Safety (pISSf) and Input-to-State Stability (ISSt) criteria to design the closed-loop control gains. The gains here are chosen such that conditions in Theorem 1 (22)-(25) and conditions in Theorem 2 (39)-(41) are satisfied for unsafe temperature specified as $T > 313K$.

The temperature response and control variables under no-anomaly scenario are shown in Figs. 3 - 5. As we can see, under nominal no-anomaly scenario the temperature dynamics in Fig. 3 remains within safe temperature zone of $T \leq 313K$ and is also stable for all three strategies: OC, St-C, and StSf-C. The measured temperature of the battery module from the two boundaries and mid-section, as shown in Fig. 5, also confirms the safety and stability of all three

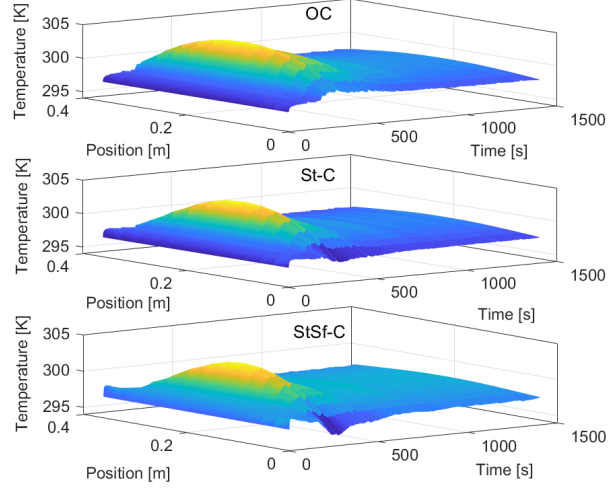


Figure 3: Spatiotemporal temperature distribution in the battery module under no-anomaly scenarios with Open-loop Control (OC), Stability-Only Control (St-C), and Stability-and-Safety Control (StSf-C).

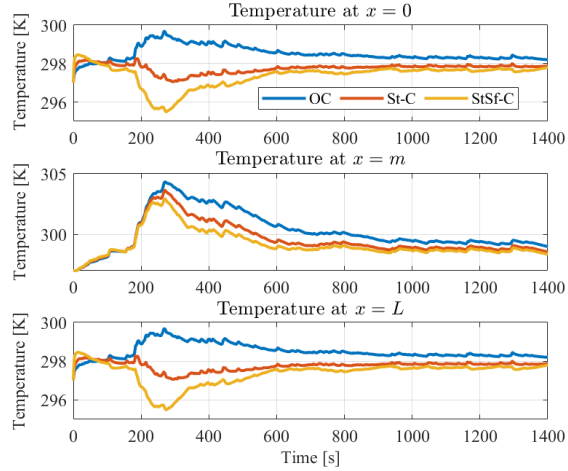


Figure 4: Temperature measurement at the two boundaries and the mid-section from the battery module under no-anomaly scenarios with Open-loop Control (OC), Stability-Only Control (St-C), and Stability-and-Safety Control (StSf-C).

strategies. In Fig. 5, the coolant temperature control at the boundaries show that the transient control action for StSf-C is greater than St-C, which in turn is greater than OC. However, in steady state all three control actions are comparable. Next, we present two test cases to illustrate the performance of the proposed approach.

5.1 Test Case I - Performance under physical fault

In this test case, we consider the scenario where the last battery cell of the module at $x = L$ is under a physical fault due to mechanical abuse/deformation. Under such scenario, local heat generation is observed in cells due to internal micro-shorts [68]. In this case study, we consider a step-like increase in heat generation of $\Delta = 10.0281J$ at $700s$ due to a mechanical fault in the last battery cell at $x = L$.

The temperature response and control variables under the three control strategies are shown in Figs. 6-8. Fig. 6 shows the spatiotemporal temperature distribution in all three cases and depicts a rapid increase in temperature at the end boundary of the battery module after $700s$. This is due to the described mechanical stress and developed micro-short inside that cell. We note that with both OC and St-C, the temperature goes to the unsafe region along the end edge of the battery, while with StSf-C the temperature continues to remain within the safe zone along the whole length of the

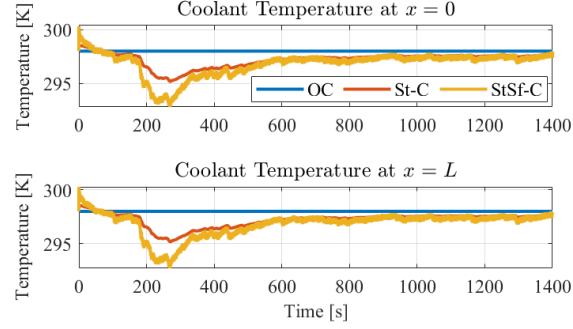


Figure 5: Coolant temperatures at the two boundaries of the battery module under no-anomaly scenarios with Open-loop Control (OC), Stability-Only Control (St-C), and Stability-and-Safety Control (StSf-C).

battery. This can be observed clearly in Fig. 7, which shows the measurement of temperature of the battery module from the front and end boundaries in addition to a middle point. The unsafe zone is shown as the grey area in the temperature plot in Fig. 7. Even though the temperature remains safe for all three strategies at $x = 0$, the temperatures at $x = L$ under OC and St-C, and the temperature at $x = m$ under OC cross into the unsafe temperature zones. However, it is clear that the temperatures remain below unsafe zone at all times along the whole length of the module for the proposed StSf-C method. This result shows that the StSf-C can be potentially beneficial to keep the temperatures under safe limits while the St-C and OC strategies may fail to achieve the same.

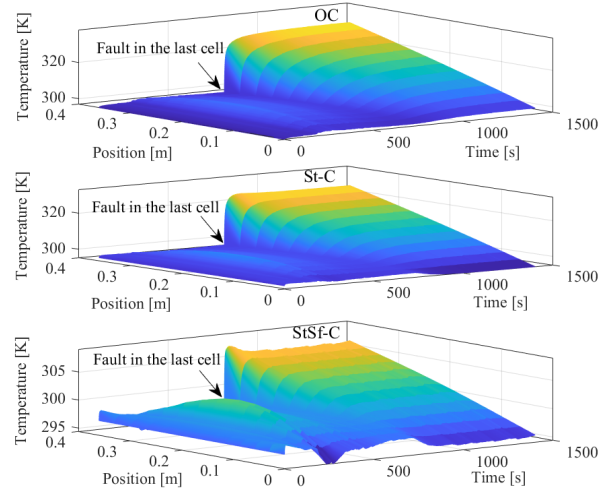


Figure 6: Spatiotemporal temperature distribution in the battery module under a faulty battery cell in the module with Open-loop Control (OC), Stability-Only Control (St-C), and Stability-and-Safety Control (StSf-C).

We note in Fig. 8 that the coolant temperature at $x = 0$ is comparable in the St-C and StSf-C scenarios while the coolant temperature is vastly decreased for StSf-C scenario at $x = L$ to counteract the fault in the battery module at $x = L$. Such drastic control action ensures that the stability condition is satisfied using our proposed strategy.

5.2 Test Case II - Performance under cyber-attack

In the second case study, we consider a scenario where an adversary injects a cyberattack to the battery module to induce overdischarge. The attack is injected at 700s as *current drain* from the module which forces the State-of-Charge (SOC) of the battery to reach zero. The SOC evolution under nominal scenario and under attack are shown in Fig. 9. It can be seen that the attack was initiated around 700s, and consequently, after 1098s the modules goes into the overdischarge mode by crossing zero SOC. Furthermore, the overdischarge proceeds to induce a battery failure through increased heating of the cell [69]. The increased heat generation due to additional current drain and subsequent heating due to overdischarge is shown in Fig. 10.

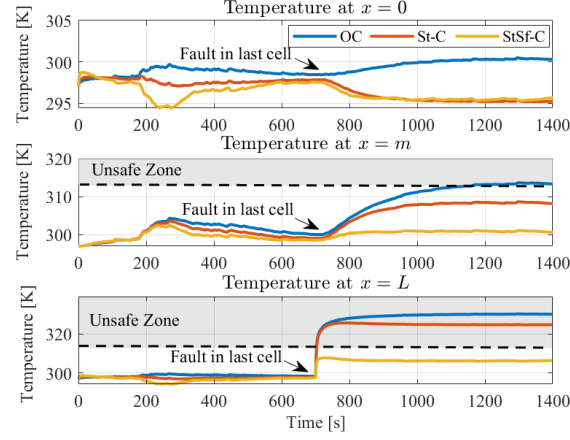


Figure 7: Temperature measurement at the two boundaries and the mid-section from the battery module under a faulty battery cell in the module with Open-loop Control (OC), Stability-Only Control (St-C), and Stability-and-Safety Control (StSf-C).

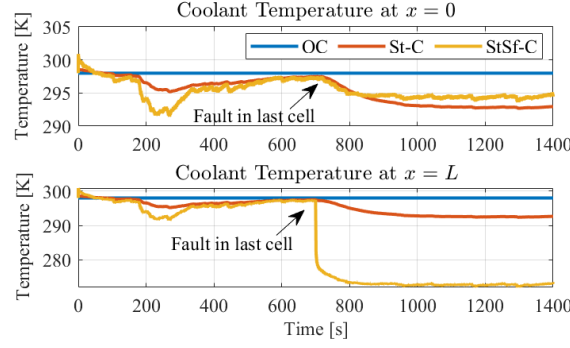


Figure 8: Coolant temperatures at the two boundaries of the battery module under a faulty battery cell in the module with Open-loop Control (OC), Stability-Only Control (St-C), and Stability-and-Safety Control (StSf-C).

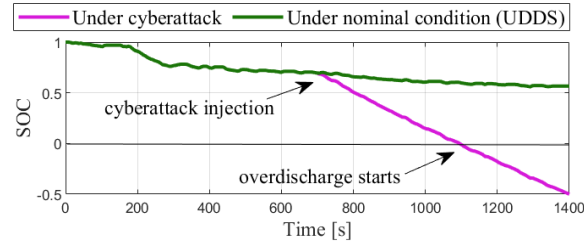


Figure 9: State-of-Charge (SOC) of the battery module under nominal condition and under cyberattack through battery overdischarge.

Next, we present the temperature response and control variables under the three control strategies are shown in Figs. 11-13. The spatiotemporal temperature distribution of the battery module in Fig. 11 shows an increased in temperature at 700s for all three strategies after the attack injection by the adversary and a further rise in temperature after the overdischarge is initiated in the module. However, only with StSf-C scheme the temperature of the module remains under the unsafe zone while temperatures reach unsafe values for both OC and Sf-C. This is again corroborated by the measurement plots in Fig. 12. The unsafe zone is again shown as the grey area in the temperature plot in Fig. 12. Even though the temperatures at $x = 0$ and $x = L$, remain in the safe zone for all three strategies, the temperature measurement from the midpoint of the battery clearly shows that OC and St-C strategies have violated the safety condition while SfSt-C were able to maintain the battery module temperature under allowable maximum of 313K. This result also shows the potential benefits of StSf-C.

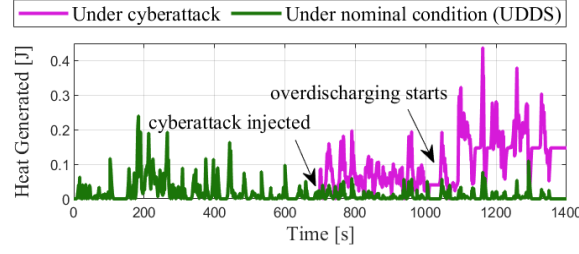


Figure 10: Heat generated in the battery module under nominal condition and under cyberattack through battery overdischarge.

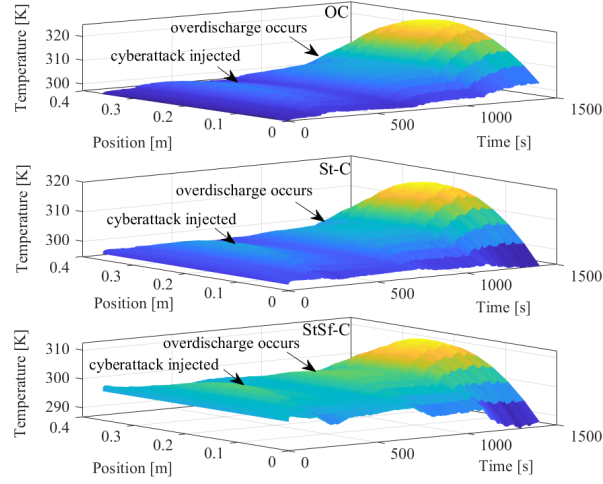


Figure 11: Spatiotemporal temperature distribution in the battery module under overdischarge cyberattack with Open-loop Control (OC), Stability-Only Control (St-C), and Stability-and-Safety Control (StSf-C).

We also note here, that the control actions presented in Fig. 13 in terms of the decrease in coolant temperature. Although the coolant temperature is successively decreased with each increase in heat generation in the battery module (once at attack injection and then with the initiation of overdischarge), the temperature of the coolant remains above sub-zero level which can be reasonably implemented in practice.

6 Conclusion

In this paper, we have explored anomaly-resilient control of DPCPSs modelled by a class of linear Parabolic PDEs with boundary control inputs. The anomalies considered are both physical faults in the system as well as corruption of system inputs through cyber-attacks on communication channel between the physical plant and central management system. First, we defined unsafe sets and distance of the system states from such unsafe sets. Next, we constructed both control barrier and Lyapunov functional in order to develop a design framework for the controller under specific safety and stability guarantees. Additionally, we have applied our proposed strategy in the context of thermal-anomaly resilient battery management system using boundary coolant control. We present the efficacy of our proposed methodologies through extensive simulation studies under both physical faults and cyber-attacks for thermal management of battery modules. The simulation study shows that the proposed approach can be beneficial to maintain safety limits. As a future work, we plan to extend the framework to a n -dimensional PDE system and apply it towards thermal management of large-scale battery packs.

References

- [1] E. D. Sontag, “Input to state stability: Basic concepts and results,” in *Nonlinear and optimal control theory*, pp. 163–220, Springer, 2008.

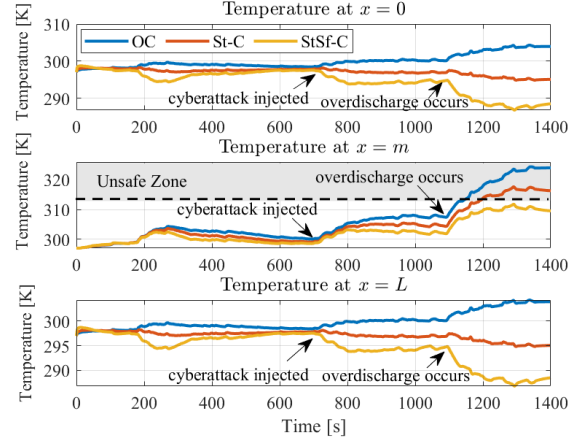


Figure 12: Temperature measurement at the two boundaries and the mid-section from the battery module under overdischarge cyberattack with Open-loop Control (OC), Stability-Only Control (St-C), and Stability-and-Safety Control (StSf-C).

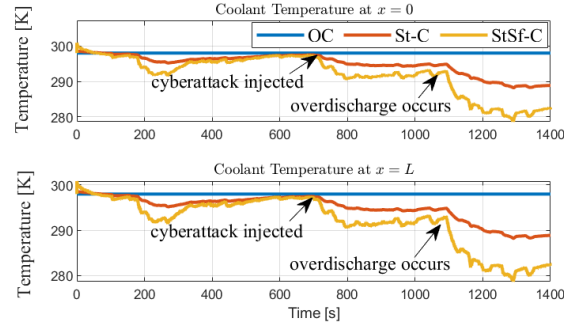


Figure 13: Coolant temperatures at the two boundaries of the battery module under overdischarge cyberattack in the module with Open-loop Control (OC), Stability-Only Control (St-C), and Stability-and-Safety Control (StSf-C).

- [2] H. Guéguen, M.-A. Lefebvre, J. Zaytoon, and O. Nasri, “Safety verification and reachability analysis for hybrid systems,” *Annual Reviews in Control*, vol. 33, no. 1, pp. 25–36, 2009.
- [3] E. D. Sontag and Y. Wang, “New characterizations of input-to-state stability,” *IEEE transactions on automatic control*, vol. 41, no. 9, pp. 1283–1294, 1996.
- [4] P. Wieland and F. Allgöwer, “Constructive safety using control barrier functions,” *IFAC Proceedings Volumes*, vol. 40, no. 12, pp. 462–467, 2007. 7th IFAC Symposium on Nonlinear Control Systems.
- [5] D. Limon, T. Alamo, D. M. Raimondo, D. M. De La Peña, J. M. Bravo, A. Ferramosca, and E. F. Camacho, “Input-to-state stability: a unifying framework for robust model predictive control,” in *Nonlinear model predictive control*, pp. 1–26, Springer, 2009.
- [6] D. Angeli and D. Efimov, “Characterizations of input-to-state stability for systems with multiple invariant sets,” *IEEE Transactions on Automatic Control*, vol. 60, no. 12, pp. 3242–3256, 2015.
- [7] D. Coutinho and C. E. de Souza, “Nonlinear state feedback design with a guaranteed stability domain for locally stabilizable unstable quadratic systems,” *IEEE Transactions on Circuits and Systems I: Regular Papers*, vol. 59, no. 2, pp. 360–370, 2011.
- [8] S. Kolathaya and A. D. Ames, “Input-to-state safety with control barrier functions,” *IEEE control systems letters*, vol. 3, no. 1, pp. 108–113, 2018.
- [9] X. Xu, P. Tabuada, J. W. Grizzle, and A. D. Ames, “Robustness of control barrier functions for safety critical control,” *IFAC-PapersOnLine*, vol. 48, no. 27, pp. 54–61, 2015.
- [10] A. G. Wills and W. P. Heath, “Barrier function based model predictive control,” *Automatica*, vol. 40, no. 8, pp. 1415–1422, 2004.

- [11] A. Taylor, A. Singletary, Y. Yue, and A. Ames, “Learning for safety-critical control with control barrier functions,” in *Learning for Dynamics and Control*, pp. 708–717, PMLR, 2020.
- [12] M. Z. Romdlony and B. Jayawardhana, “On the new notion of input-to-state safety,” in *2016 IEEE 55th Conference on Decision and Control (CDC)*, pp. 6403–6409, IEEE, 2016.
- [13] M. Z. Romdlony and B. Jayawardhana, “Stabilization with guaranteed safety using control lyapunov–barrier function,” *Automatica*, vol. 66, pp. 39–47, 2016.
- [14] A. Mironchenko and C. Prieur, “Input-to-state stability of infinite-dimensional systems: recent results and open questions,” *SIAM Review*, vol. 62, no. 3, pp. 529–614, 2020.
- [15] S. Dashkovskiy and A. Mironchenko, “On the uniform input-to-state stability of reaction-diffusion systems,” in *49th IEEE Conference on Decision and Control (CDC)*, pp. 6547–6552, IEEE, 2010.
- [16] A. Tanwani, C. Prieur, and S. Tarbouriech, “Disturbance-to-state stabilization and quantized control for linear hyperbolic systems,” *arXiv preprint arXiv:1703.00302*, 2017.
- [17] T. Roy and S. Dey, “Secure traffic networks in smart cities: Analysis and design of cyber-attack detection algorithms,” in *2020 American Control Conference (ACC)*, pp. 4102–4107, IEEE, 2020.
- [18] T. Roy and S. Dey, “Security of distributed parameter cyber-physical systems: Cyber-attack detection in linear parabolic pdes,” *arXiv preprint arXiv:2107.14159*, 2021.
- [19] I. Karafyllis and M. Krstic, “Iss with respect to boundary disturbances for 1-d parabolic pdes,” *IEEE Transactions on Automatic Control*, vol. 61, no. 12, pp. 3712–3724, 2016.
- [20] A. Mironchenko, I. Karafyllis, and M. Krstic, “Monotonicity methods for input-to-state stability of nonlinear parabolic pdes with boundary disturbances,” *SIAM Journal on Control and Optimization*, vol. 57, no. 1, pp. 510–532, 2019.
- [21] P. Pepe, I. Karafyllis, and Z.-P. Jiang, “On the liapunov–krasovskii methodology for the iss of systems described by coupled delay differential and difference equations,” *Automatica*, vol. 44, no. 9, pp. 2266–2273, 2008.
- [22] F. B. Argomedeo, C. Prieur, E. Witrant, and S. Brémond, “A strict control lyapunov function for a diffusion equation with time-varying distributed coefficients,” *IEEE Transactions on Automatic Control*, vol. 58, no. 2, pp. 290–303, 2012.
- [23] A. Mironchenko, “Criteria for input-to-state practical stability,” *IEEE Transactions on Automatic Control*, vol. 64, no. 1, pp. 298–304, 2018.
- [24] M. Ahmadi, G. Valmorbida, and A. Papachristodoulou, “Safety verification for distributed parameter systems using barrier functionals,” *Systems & Control Letters*, vol. 108, pp. 33–39, 2017.
- [25] P. D. Christofides and P. Daoutidis, “Feedback control of hyperbolic pde systems,” *AIChE Journal*, vol. 42, no. 11, pp. 3063–3086, 1996.
- [26] M. Krstic and A. Smyshlyaev, “Backstepping boundary control for first-order hyperbolic pdes and application to systems with actuator and sensor delays,” *Systems & Control Letters*, vol. 57, no. 9, pp. 750–758, 2008.
- [27] M. Krstic and A. Smyshlyaev, *Boundary control of PDEs: A course on backstepping designs*. SIAM, 2008.
- [28] A. Smyshlyaev and M. Krstic, *Adaptive control of parabolic PDEs*. Princeton University Press, 2010.
- [29] P. D. Christofides, R. Scattolini, D. Muñoz de la Peña, and J. Liu, “Distributed model predictive control: A tutorial review and future research directions,” *Computers & Chemical Engineering*, vol. 51, pp. 21–41, 2013. CPC VIII.
- [30] I. Karafyllis, N. Bekiaris-Liberis, and M. Papageorgiou, “Feedback control of nonlinear hyperbolic pde systems inspired by traffic flow models,” *IEEE Transactions on Automatic Control*, vol. 64, no. 9, pp. 3647–3662, 2018.
- [31] M. A. Demetriou, K. Ito, and R. C. Smith, “Adaptive monitoring and accommodation of nonlinear actuator faults in positive real infinite dimensional systems,” *IEEE Transactions on Automatic Control*, vol. 52, no. 12, pp. 2332–2338, 2007.
- [32] S. Ghantasala and N. H. El-Farra, “Robust actuator fault isolation and management in constrained uncertain parabolic pde systems,” *Automatica*, vol. 45, no. 10, pp. 2368–2373, 2009.
- [33] J. Cai, H. Ferdowsi, and J. Sarangapani, “Model-based fault detection, estimation, and prediction for a class of linear distributed parameter systems,” *Automatica*, vol. 66, pp. 122–131, 2016.
- [34] S. Dey, H. E. Perez, and S. J. Moura, “Robust fault detection of a class of uncertain linear parabolic pdes,” *Automatica*, vol. 107, pp. 502–510, 2019.
- [35] T. Roy, S. Sattarzadeh, and S. Dey, “Cyber-attack detection in socio-technical transportation systems exploiting redundancies between physical and social data,” *arXiv preprint arXiv:2103.11422*, 2021.

- [36] M. A. Demetriou and M. M. Polycarpou, "Incipient fault diagnosis of dynamical systems using online approximators," *IEEE Transactions on Automatic Control*, vol. 43, no. 11, pp. 1612–1617, 1998.
- [37] M. A. Demetriou, "Detection of communication attacks on spatially distributed systems with multiple interconnected actuator/sensor pairs," in *2018 IEEE Conference on Decision and Control (CDC)*, pp. 2896–2901, IEEE, 2018.
- [38] F. Fischer and J. Deutscher, "Fault diagnosis for linear heterodirectional hyperbolic ode–pde systems using backstepping-based trajectory planning," *Automatica*, vol. 135, p. 109952, 2022.
- [39] F. Fischer and J. Deutscher, "Flatness-based algebraic fault diagnosis for distributed-parameter systems," *Automatica*, vol. 117, p. 108987, 2020.
- [40] Y. Feng, Y. Wang, J.-W. Wang, and H.-X. Li, "Backstepping-based distributed abnormality localization for linear parabolic distributed parameter systems," *Automatica*, vol. 135, p. 109930, 2022.
- [41] N. H. El-Farra, "Integrated fault detection and fault-tolerant control architectures for distributed processes," *Industrial & engineering chemistry research*, vol. 45, no. 25, pp. 8338–8351, 2006.
- [42] M. Mahmood and P. Mhaskar, "Safe-parking framework for fault-tolerant control of transport- reaction processes," *Industrial & engineering chemistry research*, vol. 49, no. 9, pp. 4285–4296, 2010.
- [43] N. El-Farra, "Integrating model-based fault detection and fault-tolerant control of distributed processes," in *2006 American Control Conference*, pp. 6 pp.–, 2006.
- [44] Y. Zhang, J. Liu, and W. He, "Adaptive fault-tolerant control for a nonlinear flexible aircraft wing system," *Asian Journal of Control*, vol. 21, no. 5, pp. 2340–2351, 2019.
- [45] S. Li, W. Kang, and D.-W. Ding, "Observer-based fuzzy fault-tolerant control for nonlinear parabolic pdes," *International Journal of Fuzzy Systems*, vol. 22, no. 1, pp. 111–121, 2020.
- [46] Y. Xu, H. Yang, and B. Jiang, "Fault-tolerant control for a class of linear interconnected hyperbolic systems by boundary feedback," *Journal of the Franklin Institute*, vol. 356, no. 11, pp. 5630–5651, 2019.
- [47] Y. Guan, H. Yang, and B. Jiang, "Fault-tolerant control for a class of switched parabolic systems," *Nonlinear Analysis: Hybrid Systems*, vol. 32, pp. 214–227, 2019.
- [48] Z. Zhao, Z. Liu, W. He, K.-S. Hong, and H.-X. Li, "Boundary adaptive fault-tolerant control for a flexible timoshenko arm with backlash-like hysteresis," *Automatica*, vol. 130, p. 109690, 2021.
- [49] S. Ghantasala and N. H. El-Farra, "Active fault-tolerant control of sampled-data nonlinear distributed parameter systems," *International Journal of Robust and Nonlinear Control*, vol. 22, no. 1, pp. 24–42, 2012.
- [50] D. Zhao, B. Jiang, and H. Yang, "Backstepping-based decentralized fault-tolerant control of hypersonic vehicles in pde-ode form," *IEEE Transactions on Automatic Control*, 2021.
- [51] "Gm's future electric vehicles to debut first wireless battery management system; developed in collaboration with analog devices," 2020. <https://www.greencarcongress.com/2020/09/20200910-wbms.html>, last accessed on 12/09/21.
- [52] "Battery in the cloud." <https://www.bosch-mobility-solutions.com/en/solutions/software-and-services/battery-in-the-cloud/>, last accessed on 12/09/21.
- [53] S. Dey, Y. Shi, K. Smith, and M. Khanra, "Safer batteries via active fault tolerant control," in *2019 American Control Conference (ACC)*, pp. 1561–1566, 2019.
- [54] E. Kim, K. G. Shin, and J. Lee, "Real-time battery thermal management for electric vehicles," in *2014 ACM/IEEE International Conference on Cyber-Physical Systems (ICCPS)*, pp. 72–83, 2014.
- [55] Y. Liu and J. Zhang, "Self-adapting j-type air-based battery thermal management system via model predictive control," *Applied Energy*, vol. 263, p. 114640, 2020.
- [56] X. Tao and J. Wagner, "A thermal management system for the battery pack of a hybrid electric vehicle: modeling and control," *Proceedings of the Institution of Mechanical Engineers, Part D: Journal of Automobile Engineering*, vol. 230, no. 2, pp. 190–201, 2016.
- [57] H. Wang, F. He, and L. Ma, "Experimental and modeling study of controller-based thermal management of battery modules under dynamic loads," *International Journal of Heat and Mass Transfer*, vol. 103, pp. 154–164, 2016.
- [58] Y. Chung and M. S. Kim, "Thermal analysis and pack level design of battery thermal management system with liquid cooling for electric vehicles," *Energy conversion and management*, vol. 196, pp. 105–116, 2019.
- [59] G. Karimi and X. Li, "Thermal management of lithium-ion batteries for electric vehicles," *International Journal of Energy Research*, vol. 37, no. 1, pp. 13–24, 2013.

- [60] S. Chen, C. Wan, and Y. Wang, "Thermal analysis of lithium-ion batteries," *Journal of power sources*, vol. 140, no. 1, pp. 111–124, 2005.
- [61] D. Kato and S. J. Moura, "1d pde model for thermal dynamics in fluid-cooled battery packs: Numerical methods and sensor placement," in *2021 American Control Conference (ACC)*, pp. 3102–3107, 2021.
- [62] T. M. Bandhauer, S. Garimella, and T. F. Fuller, "A critical review of thermal issues in lithium-ion batteries," *Journal of the Electrochemical Society*, vol. 158, no. 3, p. R1, 2011.
- [63] D. H. Doughty and E. P. Roth, "A general discussion of li ion battery safety," *The Electrochemical Society Interface*, vol. 21, no. 2, p. 37, 2012.
- [64] C. Hendricks, N. Williard, S. Mathew, and M. Pecht, "A failure modes, mechanisms, and effects analysis (fmmea) of lithium-ion batteries," *Journal of Power Sources*, vol. 297, pp. 113–120, 2015.
- [65] A. Mironchenko and F. Wirth, "Characterizations of input-to-state stability for infinite-dimensional systems," *IEEE Transactions on Automatic Control*, vol. 63, no. 6, pp. 1692–1707, 2017.
- [66] H.-J. Kretzschmar and W. Wagner, "Tables of the properties of water and steam," in *International Steam Tables*, pp. 173–344, Springer, 2019.
- [67] A. Bejan, *Convection heat transfer*. John wiley & sons, 2013.
- [68] C. Zhang, S. Santhanagopalan, M. A. Sprague, and A. A. Pesaran, "Coupled mechanical-electrical-thermal modeling for short-circuit prediction in a lithium-ion cell under mechanical abuse," *Journal of Power Sources*, vol. 290, pp. 102–113, 2015.
- [69] D. Ouyang, M. Chen, J. Liu, R. Wei, J. Weng, and J. Wang, "Investigation of a commercial lithium-ion battery under overcharge/over-discharge failure conditions," *RSC advances*, vol. 8, no. 58, pp. 33414–33424, 2018.